Lawrence Berkeley National Laboratory

Title
Spin-orbit coupling driven orbital-selective doping effect in Sr2Ru1−xIrxO4

Authors
Kwon, Junyoung
Kim, Beom Seo
Kim, Mi Kyung
et al.

Peer reviewed

Spin-orbit coupling driven orbital-selective doping effect in $Sr_2Ru_{1-x}Ir_xO_4$

Junyoung Kwon,[1,2] Beom Seo Kim,[1,2] Mi Kyung Kim,[1,2] Jonathan Denlinger,[3] Aaron Bostwick,[3] Eli Rotenberg [©],[3] Nara Lee,[4]
Hwan Young Choi,[4] Jae Young Moon,[4] Young Jai Choi,[4] Junsik Mun,[1,5] Miyoung Kim,[1,5] Yoshiyuki Yoshida,[6]
Wonshik Kyung [©],[1,2,*] and Changyoung Kim[1,2,†]

[1]*Center for Correlated Electron Systems, Institute for Basic Science, Seoul 08826, Korea*
[2]*Department of Physics and Astronomy, Seoul National University, Seoul 08826, Korea*
[3]*Advanced Light Source, Lawrence Berkeley National Laboratory, Berkeley, California 94720, USA*
[4]*Department of Physics, Yonsei University, Seoul 03722, Korea*
[5]*Department of Materials Science and Engineering and Research Institute of Advanced Materials,*
Seoul National University, Seoul 08826, Korea
[6]*National Institute of Advanced Industrial Science and Technology, Tsukuba 305-8568, Japan*

Orbital-selective phenomena in mutliorbital systems have received much attention due to their uniqueness as well as possible connections to other phenomena. As orbital-selectiveness is mostly related to the crystal structure, finding a new control parameter other than structure would be of significant importance. Here we report discovery of an orbital-selective doping effect in $Sr_2Ru_{1-x}Ir_xO_4$ (SRIO). Our systematic electronic structure study of SRIO reveals an anomalous orbital-selective doping effect and concomitant Lifshitz transitions (LTs) in the γ band. With the help of a tight-binding calculation, we find that the orbital-selective doping effect is due to variation in the spin-orbit coupling (SOC) strength. Our findings not only elucidate the mechanism of LTs in the γ band in SRIO but may also open new avenues for novel SOC-controlled orbital-selective phenomena.

Orbital-selective phenomena are one of the most fascinating subjects in mutliorbital systems since their dual nature may bring about unexpected novel phenomena. The proposal that an orbital-selective Mott phase (OSMP) exists in $Sr_{2-x}Ca_xRuO_4$ (CSRO) initiated research on orbital-selective phenomena [1], and there have been numerous reports on the issue [2–5]. For instance, CSRO and iron-based superconductors (IBS) exhibit OSMPs in which Mott localization occurs in only one band [2,3]. Other systems, such as α-$MoCl_4$, exhibit orbital-selective magnetic moment suppression [5,6]. In most cases, the orbital-selectiveness comes from structural anisotropy or distortions. For instance, octahedral distortion-driven bandwidth reduction triggers the OSMP in CSRO, and tetrahedral bonding between iron and an anion (pnictogen/chalcogen) in IBS causes the d_{xy} band to become selectively localized. In addition, temperature-dependent dimerization results in orbital-selective magnetic moment suppression in α-$MoCl_4$. That is to say, crystal structure is thought to be the most important factor in triggering orbital-selective phenomena.

One may look for parameters other than crystal structure to trigger orbital-selective phenomena. As we will show here, spin-orbit coupling (SOC) is one such candidate. In heavy metal compounds such as $4d/5d$ transition metal oxides (TMOs), the strong SOC reconstructs the orbital eigenstates, which eventually results in unexpected novel phenomena

such as metal-insulator transition [7–10] and topological semimetallic behavior [11]. The SOC strength in $4d/5d$ TMOs (150–400 meV) [9,12] is comparable with the energy scale of crystal field splitting (a few hundreds of meV) [13–15], and therefore SOC may trigger an orbital-selective behavior in the same way that the crystal structure does.

$Sr_2Ru_{1-x}Ir_xO_4$ (SRIO) may be a suitable system to investigate the effect of SOC on the electronic structure. The end compounds of SRIO are a three-band metal (Sr_2RuO_4) and a J_{eff} insulator (Sr_2IrO_4). Substituting Ru^{4+} ($4d^4$) with Ir^{4+} ($5d^5$) in Sr_2RuO_4 changes both charge carrier density and SOC strength, leading to a complicated phase diagram [16]. Here we report an alternative orbital-selective effect in SRIO. In our electronic structure study of SRIO, we observe an unexpected orbital-selective electron doping effect as well as a two-step Lifshitz transitions (LTs) in the d_{xy} band as the Ir concentration (x) increases. With the help of our tight-binding (TB) calculations, we find that the orbital-selective doping effect is induced by the interplay between the electron doping effect and the SOC strength change due to Ir substitution. Our results not only describe how SOC modifies the electronic structure, but also suggest the importance of SOC as a control parameter for orbital-selective phenomena.

SRIO single crystals were grown using two methods: the floating zone method for Sr_2RuO_4 [17–19] and flux method for Ir doped samples [8,20,21]. The Ru and Ir concentrations were measured using energy-dispersive x-ray spectroscopy (Supplemental Material, Sec. I [22]), and they were found to be consistent with the nominal values. Angle-resolved photoemission spectroscopy (ARPES) measurements were
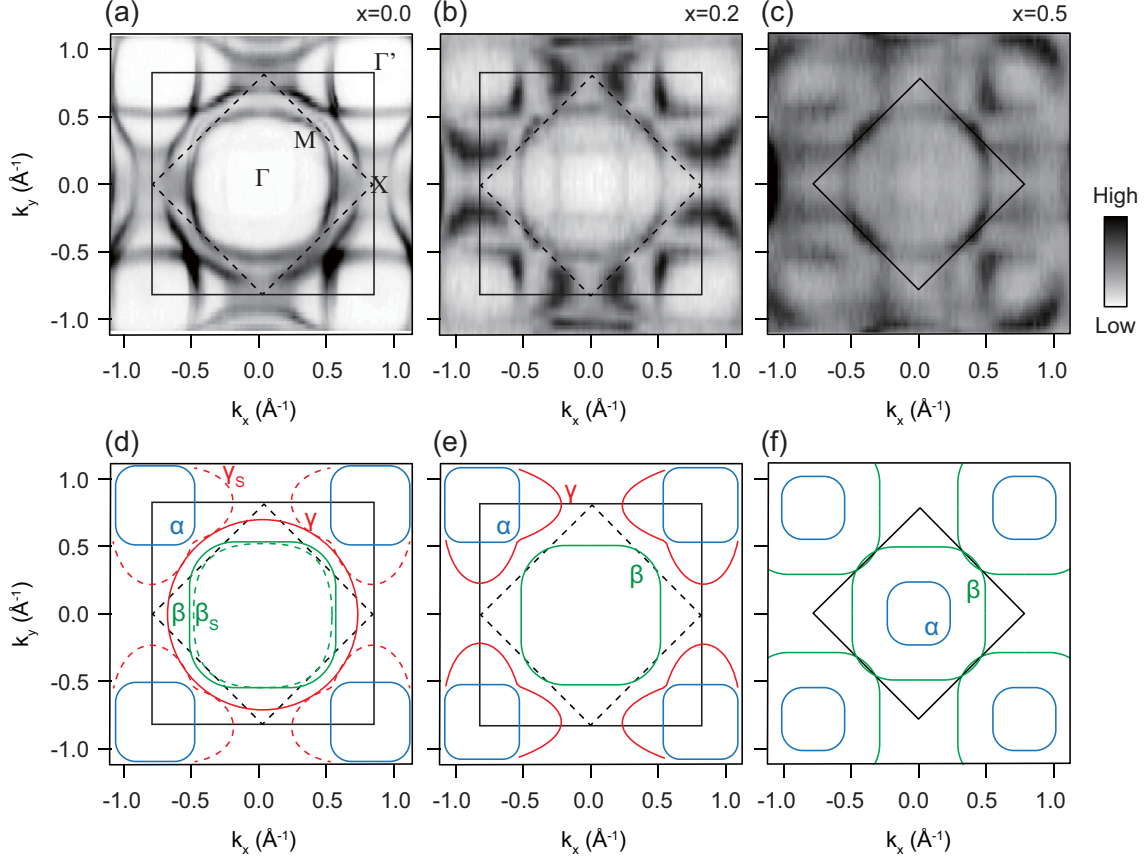
FIG. 1. Fermi surface (FS) maps for SRIO. (a)–(c) Experimental FS map for (a) $x = 0.0$, (b) 0.2, and (c) 0.5, and (d)–(f) corresponding schematic band structures. The solid black squares mark the bulk Brillouin zone (BZ) at each doping level, and dashed black ones are the $\sqrt{2} \times \sqrt{2}$ reduced BZ due to surface octahedral rotation (OR). At $x = 0.5$, there is bulk OR distortion which leads to a $\sqrt{2} \times \sqrt{2}$ reduced BZ as the surface OR does in (a) and (b). The blue, green, and red lines in panels (d)–(f) indicate α, β, and γ bands, respectively. Solid (dashed) lines correspond to bulk (surface) FS pockets. For an easier understanding, symbols of the $\sqrt{2} \times \sqrt{2}$ reduced BZ are used for high symmetry points as denoted in (a).

performed at the beamlines 4.0.3 and 7.0.2 of the Advanced Light Source, Lawrence Berkeley National Laboratory, California, USA. Samples were cleaved *in situ* and measurements were performed using $h\nu = 70$ eV light with linear horizontal polarization. More detailed description on the experimental condition is given in Sec. II of the Supplemental Material [22].

Figure 1 shows the Fermi surfaces (FSs) of SRIO. The FS of Sr$_2$RuO$_4$ [$x = 0.0$, Figs. 1(a) and 1(d)] shows three types of FS pockets (α, β, and γ) depending on orbital characters (d_{xy} for γ and $d_{yz/zx}$ for α/β) [26–28]. Octahedral rotation (OR) distortion, which exists on the surface of Sr$_2$RuO$_4$, duplicates these FS pockets (α_S, β_S, and γ_S) with a reduction of the Brillouin zone (BZ) of $\sqrt{2} \times \sqrt{2}$. Note that the bulk γ band is an electron-like pocket centered at Γ, while the surface band γ_S is a hole-like pocket centered at (π, π) of the unreduced BZ (or at Γ' of the reduced BZ). It can clearly be seen that the α/β and γ bands show completely different responses to Ir doping. As x increases, the FS volume of the α/β bands hardly changes, with an invariant FS topology. On the other hand, the (bulk) γ band shows two-step LTs around $x = 0.2$ and 0.5 [Figs. 1(e) and 1(f)].

The first LT occurs between $x = 0.1$ and $x = 0.2$ [Figs. 1(b) and 1(e)]. The γ FS exhibits an electron-like

pocket for $x < 0.2$, thus the surface distortion-driven hole-like γ_S can be distinguished [Figs. 1(a) and 1(d)]. As x increases, we observed the electron-like γ FS disappears at $x = 0.2$ while the hole-like γ becomes intensified. We obtained our FS images after aging the samples (Supplemental Material, Fig. S2 [22]) to eliminate surface-distortion-driven bands. Considering those figures, the disappearance of the electron-like γ FS is due to the first LT to a hole-like FS. As x further increases, the γ FS disappears between $x = 0.4$ and $x = 0.5$ (the second LT), leaving only the α and β FSs [Figs. 1(c) and 1(f)]. Detailed analysis are provided in Supplemental Material Fig. S3 [22]. Note that α and β hardly change, while γ shows a dramatic variation in FS topology with increasing x.

To track the x-dependent electronic structure evolution quantitatively, we extract the electron occupation number of each band using the Luttinger's theorem [Fig. 2(a)]. As mentioned above, Ir substitution for Ru changes both charge carrier density and SOC strength. If we neglect the effect of SOC, it is natural that the electron occupations of all three bands (α, β, and γ) increase with x, which is supported by TB calculations [Fig. 2(a)]. However, the estimation based on our experimental results [Fig. 2(a)] shows a totally different behavior. As x increases, the γ band fills with a larger
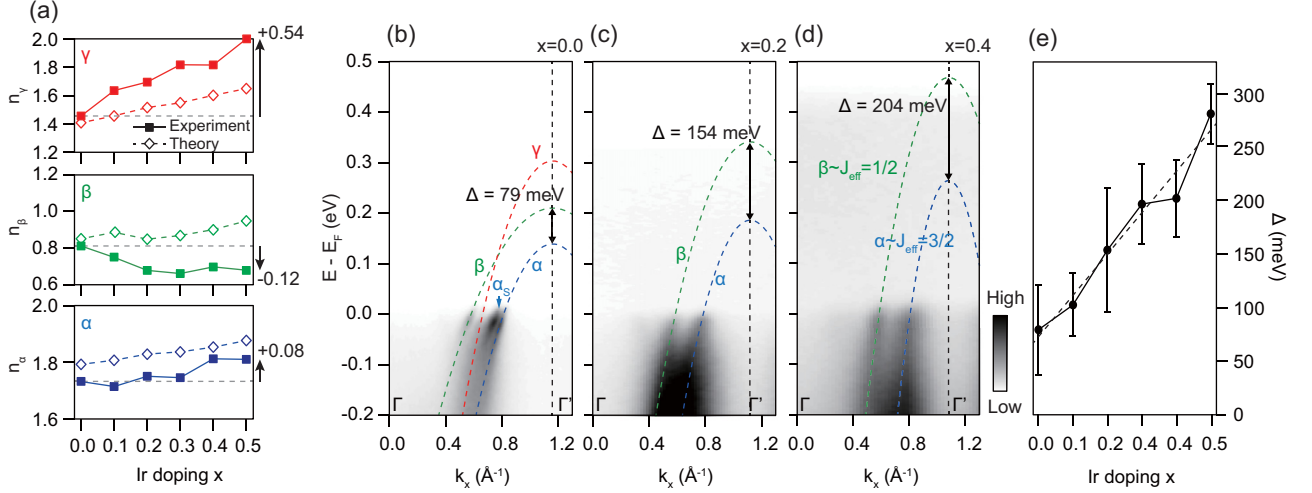
FIG. 2. (a) Experimentally (filled square) and theoretically (empty square) obtained electron occupation numbers as a function of the Ir concentration (x) for α, β, and γ bands. Due to the difficulty in tracking the γ electron occupation (n_γ), n_γ is estimated from $n_{tot} - n_\alpha - n_\beta$, and n_γ is set to be 2.0 for $x \geqslant 0.5$. The theoretical electron numbers are calculated by assuming a rigid-band-like shift in our tight-binding (TB) calculation [Fig. 3(b)]. The black arrows indicate the change of the experimental value between $x = 0.0$ and 0.5. (b–d) Band dispersions along the $\Gamma - \Gamma'$ high symmetry line for (b) $x = 0.0$, (c) 0.2, and (d) 0.4. The colored dashed lines are extrapolated (quadratic) band dispersions for the bands. The energy difference between the top of α and β bands (Δ) is expected to be proportional to the SOC strength since α (β) band corresponds to $J_{\text{eff}} = 3/2$ ($J_{\text{eff}} = 1/2$) near the Fermi energy. (e) x-dependent Δ for $x \leqslant 0.5$.

number of electrons ($0.54e$ at $x = 0.5$) compared to the theoretically estimated value ($0.24e$). Furthermore, the β band undergoes a negative electron doping effect [$n_\beta(x = 0.5) - n_\beta(x = 0.0) \approx -0.12e$], showing a deviation between the experimental and theoretical values of approximately $-0.27e$ at $x = 0.5$. In brief, as x increases from 0 to 0.5, the changes in electron numbers are $0.08e$ (α), $-0.12e$ (β), and $0.54e$ (γ). In other words, most of the electrons from Ir doping ($0.5e$ at $x = 0.5$) are selectively received by the γ band.

The observed orbital-selective doping effect can be attributed to the SOC. Ir ($\lambda_{SOC} \approx 400$ meV) substitution of Ru ($\lambda_{SOC} \approx 150$ meV) applies a stronger SOC to the electronic structure; Figs. 2(b)–2(d) show the effect. Previous studies of $4d/5d$ TMOs revealed that the SOC strongly affects the eigenstates of α, β, and γ bands [7,8,29], and it is known that the energy splitting (Δ) between α and β is proportional to the SOC strength [9,30]. In order to estimate the variation of the SOC, we extracted Δ by extrapolating the experimental bands with an assumed quadratic dispersion (Supplemental Material, Sec. III [22]). As expected, we observe an approximate proportionality between Δ and x increase [Figs. 2(b)–2(e)], which indicates that varying the SOC strength significantly modifies the electronic structure of SRIO.

The detailed role of the SOC in the electronic structure can be investigated using TB calculations. As SOC strength increases, all the bands (α, β, and γ) become mixed orbital states (near J_{eff} states). As a result, the relative energy level difference between the β and γ bands increases with SOC (black arrow on the X point in Figs. 3(a)–3(c)). The orbital-selective doping effect in Fig. 2(a) can be understood to be due to the SOC-driven splitting between the β and γ bands. The SOC moves the γ (β) band downward (upward) in terms of energy [Figs. 3(a)–3(c)], transferring electrons from β to γ. Hence, the TB calculation indicates that the orbital-selective

doping effect in γ and the negative doping effect in β can be explained by the change in SOC.

Let us reconsider the LTs in the γ band. The first LT in SRIO is analogous to that observed in a previous study on $Sr_{2-x}La_xRuO_4$ [31]. In $Sr_{2-x}La_xRuO_4$, La ($5d6s^2$) substitution of Sr ($5s^2$) applies an electron doping effect (without SOC strength change), leading to an LT in the γ band near $x = 0.27$ ($0.27e$) which accompanies a FS change from an electron- to hole-like pocket. Note that the first LT in SRIO occurs at $x < 0.2$ ($0.2e$). That is, SRIO requires a smaller electron number to generate the LT, compared to $Sr_{2-x}La_xRuO_4$. Considering that an increase in the SOC has an electron doping effect on the γ band [Figs. 3(a)–3(c) and 3(e)–3(g)], increased SOC strength leads to an additional doping effect in the γ band. Therefore, the first LT in SRIO occurs at a lower doping level ($x < 0.2$) compared to that in $Sr_{2-x}La_xRuO_4$ (near $x = 0.27$).

As for the second LT (the missing γ band at $x = 0.5$), we performed further simulation via a TB calculation. Figure 3(h) shows a simple electron doping effect on top of the strong SOC shown in Fig. 3(g). As can be seen in Fig. 3(h), the γ FS pocket still exists, even though it becomes significantly smaller. That is, the second LT cannot be fully understood by considering only the SOC and electron doping effects.

The last piece of the puzzle for the second LT is the OR distortion. A previous crystallographic study on SRIO revealed that OR appears around $x = 0.5$ [16], which we confirm again with transmission electron diffraction measurements (Supplemental Material, Sec. IV [22]). According to theoretical studies on Sr_2RhO_4 and $Sr_{2-x}Ca_xRuO_4$, OR plays a significant role in the electronic structure by causing $d_{x^2-y^2}$ and d_{xy} to hybridize and, eventually, d_{xy} (or partially mixed $d_{x^2-y^2}$) to sink below the Fermi level [32,33]. To examine the role of OR further, we performed a TB calculation which considers the OR in addition to the effect considered in Figs. 3(c) and 3(h).
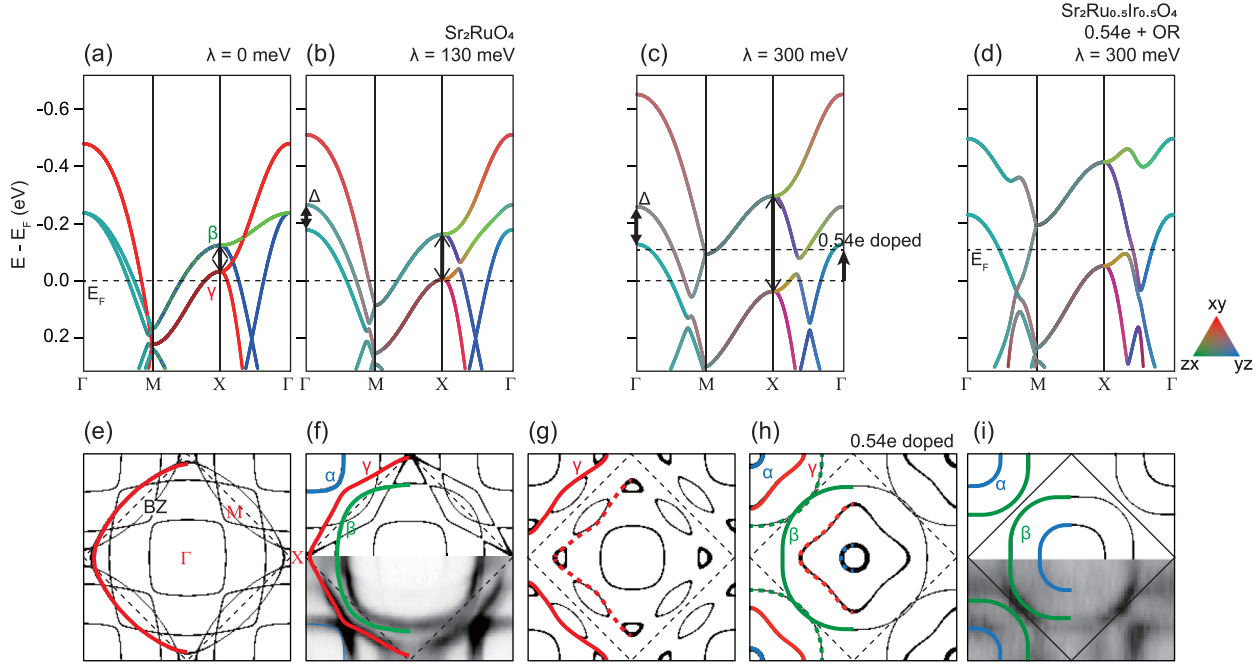
FIG. 3. (a)–(c) SOC-dependent electronic structures from TB calculations for (a) $\lambda = 0$, (b) 130, and (c) 300 meV, and (e)–(g) corresponding FS maps. Δ, the splitting between α and β bands at Γ, is defined in Fig. 2. (h) FS map of (c) ($\lambda = 300$ meV) but with 0.54 electron doping which is taken from the n_γ in Fig. 2(a). (d), (i) OR effect is further considered in addition to $\lambda = 300$ meV and 0.54 electron doping. To show the SOC-driven orbital mixing effect in panels (a)–(d), the band characters are color coded with d_{xy} (red), d_{zx} (green), and d_{yz} (blue) projection. The TB calculation results in panels (f) and (i) closely resemble the experimentally obtained FS maps of Sr_2RuO_4 [Fig. 1(a)] and $Sr_2Ru_{0.5}Ir_{0.5}O_4$ [Fig. 1(c)], respectively.

The result [Figs. 3(d) and 3(i)] successfully reproduces the missing γ FS (the second LT).

Figure 4 summarizes the electron occupation of the γ band and the electronic phase diagram (the number of FS pockets). We categorize the source of the electrons in the γ band (Fig. 4). The result shows that SOC variation leads to a large
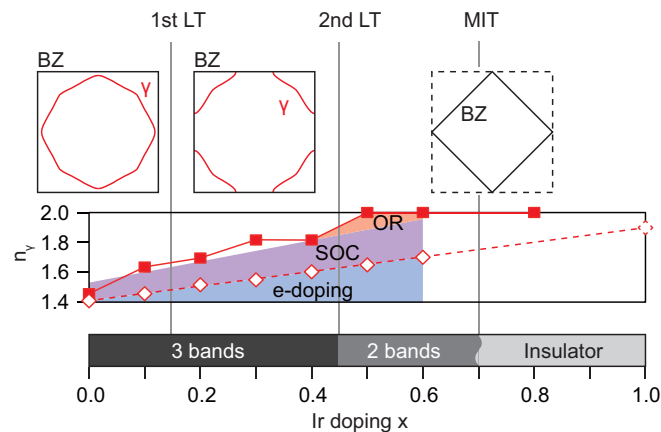

FIG. 4. Ir concentration dependent evolution of the γ band. The upper panel displays the x-dependent topology of the γ band. The corresponding electron occupation number n_γ is shown in the middle panel. Based on the TB calculation result in Fig. 3, the change in the electron number is quantitatively attributed to contributions from electron doping, SOC, and OR. On the bar in the lower panel, the doping range is categorized in terms of the number of FSs.

electron doping effect that is comparable to the "e-doping" case (the simple electron doping effect due to the number of valence electrons). Notably, the "e-doping" effect alone does not cause full occupation of the γ band even though we extrapolated up to $x = 1.0$, thus SOC is an essential ingredient to cause full occupation of γ.

At this stage, we can consider how a three-band metal (Sr_2RuO_4) evolves into a Mott insulator (Sr_2IrO_4) over the full doping range in SRIO. A previous study on $Sr_{2-x}La_xRhO_4$ revealed that the "single-band" is one of the essential conditions for a J_{eff} Mott state [10]. In this regard, to fully understand SRIO, it is important to track how the number of bands evolves. At $x = 0.0$, three FS pockets (α, β, and γ) exist because three nearly degenerate t_{2g} states are filled with four electrons. As x increases, SOC lifts the degeneracy of t_{2g}. Up to $x = 0.5$, the γ band becomes fully occupied because of the orbital-selective doping effect, and therefore the SRIO becomes a two-band metal (α and β). With further Ir doping ($x > 0.5$), the stronger SOC causes α and β to split further, and the SRIO eventually becomes single-band (β) which meets the necessary condition for a Mott state as in the Sr_2IrO_4 ($x > 0.7$, Supplemental Material, Fig. S6 [22]).

Our study of SRIO has several important implications. The first concerns the discovery of an exotic orbital-selective doping effect driven by SOC. Until now, crystal structure was thought to be the most important factor to trigger orbital-selective phenomena. However, the energy scales of SOC strength (150–400 meV in $4d/5d$ TMOs) [9,12] are comparable with that of crystal field splitting (a few hundreds of meV)

[13–15], and thus the SOC may be a factor that is sufficient to trigger orbital-selective phenomena. Consistent with this, we observe an orbital-selective doping effect in SRIO that is driven by SOC variation, thus our study may expand the boundary of orbital-selective physics to materials in the strong SOC regime.

Another importance of our study is the provision of quantitative analysis on the role of SOC. Although there have been many studies of $5d$ iridates, which have strong SOC, most were limited to the strong SOC regime, focusing on the exotic phenomena of the system itself. For instance, there have been various electronic structure studies of SRIO as well as $Sr_2Rh_{1-x}Ir_xO_4$ to understand the role of SOC [30,34,35], but most have focused on the strong SOC-driven Mott insulating state in Sr_2IrO_4, not on how SOC determines the electronic structures. Furthermore, in the case of $Sr_2Rh_{1-x}Ir_xO_4$, whether the effective SOC strength actually changes with the Rh concentration is still controversial [34–37]. Therefore, to understand the role of SOC fully, appropriate target materials (such as SRIO) as well as quantitative/comprehensive studies that track the electronic structure evolution with SOC is essential. To achieve this goal, it is highly required to investigate the electronic structure of the metallic state side rather than the insulating one, because the strong electron correlation effect precludes observing the electronic structure directly. In this respect, we focus on the metallic state of SRIO, which shows apparent x-dependent effective SOC variation (Fig. 2), and we quantitatively extract the effects of SOC in terms of electron redistribution in the electronic structure. We believe that our study not only elucidates how SOC transforms the electronic structure sufficiently to form the Mott state in SRIO but also provides a methodological way to estimate the effect of SOC quantitatively.

In conclusion, we performed systematic electronic structure studies of SRIO and found an alternative orbital-selective doping effect. From the quantitative analysis of our ARPES results with the help of TB simulation, we found that the SOC in SRIO reconstructs the band structure, which eventually leads to the orbital-selective doping effect on γ. Our findings not only elucidate the mechanism of LTs in the γ band in SRIO but also may open new avenues for novel SOC-controlled orbital-selective phenomena.

[1] V. I. Anisimov, I. A. Nekrasov, D. E. Kondakov, T. M. Rice, and M. Sigrist, Eur. Phys. J. B **25**, 191 (2002).

[2] M. Neupane, P. Richard, Z.-H. Pan, Y.-M. Xu, R. Jin, D. Mandrus, X. Dai, Z. Fang, Z. Wang, and H. Ding, Phys. Rev. Lett. **103**, 097001 (2009).

[3] M. Yi, Z.-K. Liu, Y. Zhang, R. Yu, J.-X. Zhu, J. J. Lee, R. G. Moore, F. T. Schmitt, W. Li, S. C. Riggs, J.-H. Chu *et al.*, Nat. Commun. **6**, 7777 (2015).

[4] S. Hoshino and P. Werner, Phys. Rev. Lett. **118**, 177002 (2017).

[5] D. M. Korotin, V. I. Anisimov, and S. V. Streltsov, Sci. Rep. **6**, 25831 (2016).

[6] S. V. Streltsova and D. I. Khomskii, Phys. Usp. **60**, 1121 (2017).

[7] B. J. Kim, H. Jin, S. J. Moon, J.-Y. Kim, B.-G. Park, C. S. Leem, J. Yu, T. W. Noh, C. Kim, S.-J. Oh *et al.*, Phys. Rev. Lett. **101**, 076402 (2008).

[8] B. J. Kim, H. Ohsumi, T. Komesu, S. Sakai, T. Morita, H. Takagi, and T. Arima, Science **323**, 1329 (2009).

[9] M. W. Haverkort, I. S. Elfimov, L. H. Tjeng, G. A. Sawatzky, and A. Damascelli, Phys. Rev. Lett. **101**, 026406 (2008).

[10] J. Kwon, M. Kim, D. Song, Y. Yoshida, J. D. Denlinger, W. Kyung, and C. Kim, Phys. Rev. Lett. **123**, 106401 (2019).

[11] K. Ueda, R. Kaneko, H. Ishizuka, J. Fujioka, N. Nagaosa, and Y. Tokura, Nat. Commun. **9**, 3032 (2018).

[12] S. Zhou, K. Jiang, H. Chen, and Z. Wang, Phys. Rev. X **7**, 041018 (2017).

[13] H.-J. Noh, S.-J. Oh, B.-G. Park, J.-H. Park, J.-Y. Kim, H.-D. Kim, T. Mizokawa, L. H. Tjeng, H.-J. Lin, C. T. Chen *et al.*, Phys. Rev. B **72**, 052411 (2005).

[14] R. D. Wulandari, S. Muhammady, and Y. Darma, J. Phys. Chem. Solids **137**, 109225 (2020).

[15] S. G. Jeong, G. Han, S. Song, T. Min, A. Y. Mohamed, S. Park, J. Lee, H. Y. Jeong, Y. M. Kim, D. Y. Cho, W. S. Choi, Adv. Sci. **7**, 2001643 (2020).

[16] S. J. Yuan, S. Aswartham, J. Terzic, H. Zheng, H. D. Zhao, P. Schlottmann, and G. Cao, Phys. Rev. B **92**, 245103 (2015).

[17] S. I. Ikeda, U. Azuma, N. Shirakawa, Y. Nishihara, and Y. Maeno, J. Cryst. Growth **237–239**, 787 (2002).

[18] Z. Q. Mao, Y. Maeno, and H. Fukazawa, Mater. Res. Bull. **35**, 1813 (2000).

[19] N. Kikugawa, R. Baumbach, J. S. Brooks, T. Terashima, S. Uji, and Y. Maeno, Cryst. Growth Des. **15**, 5573 (2015).

[20] A. Glamazda, W. J. Lee, K. Y. Choi, P. Lemmens, H. Y. Choi, N. Lee, and Y. J. Choi, Phys. Rev. B **89**, 104406 (2014).

[21] Y. J. Yan, M. Q. Ren, H. C. Xu, B. P. Xie, R. Tao, H. Y. Choi, N. Lee, Y. J. Choi, T. Zhang, and D. L. Feng, Phys. Rev. X **5**, 041018 (2015).

[22] See Supplemental Material at http://link.aps.org/supplemental/10.1103/PhysRevB.103.L081104 for the EDX analysis, the details of ARPES data analysis, the TED measurement, the details of TB calculation, and the ARPES data of the higher doping rate, which includes Refs. [23–25].

[23] J. Karp, M. Bramberger, M. Grundner, U. Schollwöck, A. J. Millis, and M. Zingl, Phys. Rev. Lett. **125**, 166401 (2020).

[24] A. Damascelli, Phys. Scr. **2004**, 61 (2004).

[25] A. de la Torre, S. McKeown Walker, F. Y. Bruno, S. Riccó, Z. Wang, I. Gutierrez Lezama, G. Scheerer, G. Giriat, D. Jaccard, C. Berthod, T. K. Kim *et al.*, Phys. Rev. Lett. **115**, 176402 (2015).

[26] A. Tamai, M. Zingl, E. Rozbicki, E. Cappelli, S. Riccó, A. de la Torre, S. McKeown Walker, F. Y. Bruno, P. D. C. King, W. Meevasana *et al.*, Phys. Rev. X **9**, 021048 (2019).

[27] C. N. Veenstra, Z.-H. Zhu, B. Ludbrook, M. Capsoni, G. Levy, A. Nicolaou, J. A. Rosen, R. Comin, S. Kittaka, Y. Maeno *et al.*, Phys. Rev. Lett. **110**, 097004 (2013).

[28] A. Damascelli, D. H. Lu, K. M. Shen, N. P. Armitage, F. Ronning, D. L. Feng, C. Kim, Z.-X. Shen, T. Kimura, Y. Tokura *et al.*, Phys. Rev. Lett. **85**, 5194 (2000).

[29] C. Martins, M. Aichhorn, and L. Vaugïer, S. Biermann, Phys. Rev. Lett. **107**, 266404 (2011).

[30] B. Zwartsenberg, R. P. Day, E. Razzoli, M. Michiardi, N. Xu, M. Shi, J. D. Denlinger, G. Cao, S. Calder, K. Ueda *et al.*, Nat. Phys. **16**, 290 (2020).

[31] K. M. Shen, N. Kikugawa, C. Bergemann, L. Balicas, F. Baumberger, W. Meevasana, N. J. C. Ingle, Y. Maeno, Z.-X. Shen, and A. P. Mackenzie, Phys. Rev. Lett. **99**, 187001 (2007).

[32] B. J. Kim, J. Yu, H. Koh, I. Nagai, S. I. Ikeda, S. J. Oh, and C. Kim, Phys. Rev. Lett. **97**, 106401 (2006).

[33] E. Ko, B. J. Kim, C. Kim, and H. J. Choi, Phys. Rev. Lett. **98**, 226401 (2007).

[34] Y. Cao, Q. Wang, J. A. Waugh, T. J. Reber, H. Li, X. Zhou, S. Parham, S.-R. Park, N. C. Plumb, E. Rotenberg *et al.*, Nat. Commun. **7**, 11367 (2016).

[35] A. Louat, F. Bert, L. Serrier-Garcia, F. Bertran, P. Le Fèvre, J. Rault, and V. Brouet, Phys. Rev. B **97**, 161109(R) (2018).

[36] S. Chikara, D. Haskel, J.-H. Sim, H.-S. Kim, C.-C. Chen, G. Fabbris, L. S. I. Veiga, N. M. Souza-Neto, J. Terzic, K. Butrouna *et al.*, Phys. Rev. B **92**, 081114(R) (2015).

[37] J. Bertinshaw, J. K. Kim, J. Porras, K. Ueda, N. H. Sung, A. Efimenko, A. Bombardi, J. Kim, B. Keimer, and B. J. Kim, Phys. Rev. B **101**, 094428 (2020).